ELSEVIER

Earth and Planetary Science Letters 205 (2003) 173–184

EPSL

www.elsevier.com/locate/epsl

Low-temperature cycling of isothermal and anhysteretic remanence: microcoercivity and magnetic memory

Adrian R. Muxworthy *, David J. Dunlop, Özden Özdemir

Geophysics, Department of Physics, University of Toronto, Toronto, ON, Canada

Received 1 July 2002; received in revised form 17 October 2002; accepted 17 October 2002

Abstract

This paper reports low-temperature cycling (LTC) through the Verwey transition of anhysteretic remanence (ARM), partial ARMs and partially demagnetised saturation isothermal remanence (SIRM) induced at room temperature in pseudo-single-domain and multidomain (MD) magnetite. The remanences were cooled in zero field to 50 K and then heated back to room temperature. By inducing partial ARMs over different field ranges and by partially alternating field demagnetising SIRMs, it was possible to isolate both low-coercive-force and high-coercive-force fractions of remanence. On cooling through the Verwey transition, a sharp increase in the remanence was observed. The relative size of the jump increased as the high-coercive-force fraction was increasingly isolated. This behaviour is interpreted as being due to both an increase in the single-domain/multidomain threshold size on cooling through the Verwey transition and to the reduction or elimination of closure domains in the low-temperature phase. In addition, the memory ratio, i.e. the fraction of remanence remaining after LTC divided by the initial remanence, was found to be higher for the high-coercive-force fraction than the low-coercive-force fraction. In our interpretation, the high-coercivity fraction behaviour is associated with reversible domain re-organisation effects, whilst the low-coercive force fraction's behaviour is associated with irreversible domain re-organisation and (de-)nucleation processes. Due to the decrease in magnetocrystalline anisotropy on cooling to the Verwey transition, the high-coercive-force fraction is likely to be magnetoelastically controlled. Thus, a rock displaying high-coercive-force behaviour is likely to carry a palaeomagnetically meaningful remanence with high unblocking temperatures. In addition, LTC analysis can be used to identify the domain state dominating the natural remanence in magnetite-bearing rocks.

Keywords: magnetite; Verwey transition; domain state; coercivity; remanence

1. Introduction

Zero-field low-temperature cycling (LTC) of magnetite-bearing rocks from room temperature to liquid nitrogen temperature causes varying degrees of partial demagnetisation of remanence depending on domain state [1–8]. The partial demagnetisation is thought to be primarily related to

* Corresponding author. Present address: Department of Geology and Geophysics, University of Edinburgh, King's Buildings, West Mains Road, Edinburgh EH9 3JW, UK.
E-mail address: adrian.muxworthy@ed.ac.uk (A.R. Muxworthy).

0012-821X/02/$ – see front matter © 2002 Elsevier Science B.V. All rights reserved.
PII: S0012-821X(02)01039-7

changes in the magnetocrystalline anisotropy, but the exact processes governing LTC behaviour are still unresolved. There is a need for greater understanding if LTC is to become a reliable palaeomagnetic or environmental magnetic technique.

To understand the mechanisms controlling demagnetisation, it is revealing to study the LTC behaviour of various initial remanence states. The direct measurement of remanence during LTC has not been extensive; previous studies have predominantly considered saturation isothermal remanence (SIRM) [1–4,6–8]. It is found that SIRM induced in a multidomain (MD) sample at room temperature gradually decreases on cooling to the magnetocrystalline energy isotropic point T_K at 130 K and the Verwey transition T_V at 120–124 K [9,10]. This decrease in remanence has been associated with domain re-ordering effects, i.e. domain wall re-equilibration or domain nucleation [4,7]. On cooling through T_V, an increase in magnetisation or 'jump' is observed. The size of the jump for SIRM carried by assemblages of crystals is relatively small compared to that of SIRM induced in orientated single crystals $\sim$1–4 mm in diameter [6,8]. Below the monoclinic/triclinic phase of magnetite, SIRM displays thermally reversible behaviour. On warming through T_V, the jump is found to be mainly, though not always, reversible. On warming from T_K to room temperature, SIRM displays irreversible behaviour, with some increase in magnetisation (recovery). The degree of recovery is found to be dependent on internal stress [11] and has been associated with the stiffening of domain walls on heating [7].

There are a limited number of studies of the low-temperature cycling of thermoremanent magnetisation (TRM) [1,7,12], of which by far the most extensive is the paper of Muxworthy and McClelland [7], who measured LTC behaviour of TRM and partial TRMs (pTRMs) induced in well characterised synthetic and natural stoichiometric pseudo-single-domain (PSD) and MD magnetites. TRM and pTRM carried by assemblages of magnetite crystals consistently displayed a large jump on cooling through T_V. The size of the jump was influenced by grain size, the temperature range over which the pTRM was acquired and inducing field intensity, e.g. high-temperature pTRMs induced in small fields in PSD samples displayed larger jumps than pTRMs induced in larger fields in large MD samples at lower temperatures. The size of the jump was on average larger than that observed for the same samples carrying an SIRM [7].

In addition to experiments, micromagnetic and other numerical models of single sub-micrometre crystals predict the jump behaviour at T_V for simulated SIRM, TRM and pTRM structures [5,13]. However, due to the simplifications of the model the size of the simulated jump was larger than that observed for assemblages of small PSD magnetites.

The behaviour at T_V was explained by a shift in domain state to a more single domain-like (SD) structure and the removal of closure domains in the monoclinic phase [5,7,8]. This was concluded by examining hysteresis data, micromagnetic solutions and by considering the relative anisotropy which indicates the favourability of closure domains [5,8,14]. It was suggested that closure domains play a more important role in reducing the demagnetising energy in small grains than larger grains and in pTRM structures acquired at high temperatures.

The results of TRM LTC curves have been revealing, but our current knowledge of MD TRM acquisition is incomplete, making it difficult to fully interpret such LTC data. To quantify and improve our understanding of the behaviour of remanence at low temperatures, in this paper LTC curves of partially alternating-field (AF) demagnetised SIRM, anhysteretic remanence (ARM) and partial ARM (pARM) are presented. It is the first time LTC curves for such remanences have been reported. Although these remanences in MD magnetite are not fully understood [15], our knowledge is better than that of TRM as we can more accurately identify which part of the coercivity spectrum is affected during the induction.

2. Sample description

Magnetite samples from two different origins

were utilised in this study; three small commercial MD samples *W*(1.7 μm), *W*(7.0 μm) and *W*(11 μm), acquired from Wright Industries, and two MD synthetic samples made by hydrothermal recrystallisation (H (39 μm)) and (H (108 μm)).

The Wright samples were obtained 6 months before the experimentation and stored in a desiccator. Grain size distributions were found to be log-normal from scanning electron microscope photographs (Table 1). X-ray diffraction (XRD) spectra measured shortly after receiving the samples appeared to be those of pure magnetite within experimental limits. However, during the LTC measurements at the Institute for Rock Magnetism, spectra measured using a ^{57}Co source identified non-stoichiometric magnetite (Fig. 1). It is uncertain whether this partial oxidation occurred during the 6 months of storage or if the samples were initially non-stoichiometric.

Mössbauer parameters were determined by fitting two sextets (A and B) using a Lorentzian fitting programme (Table 2). The oxidation state of the samples was estimated by considering the ratio of the area of the two sextets (F_A and F_B). For stoichiometric magnetite the ratio is experimentally $\sim$1.9 [16]. Two possible interpretations are considered; the first is that there are two separate phases within the sample, i.e. a stoichiometric maghemite phase and a stoichiometric magnetite phase. The second interpretation is that the samples are homogeneous cation-deficient magnetite with a formula given by $Fe^{3+}_{2+2z/3}Fe^{2+}_{1-z}\square_{z/3}O_4$, $0 \leq z \leq 1$, where $\square$ = cation vacancy. In reality it is likely that neither model is correct and the mineralogy is a mixture of both. It is possible to differentiate between two such configurations by

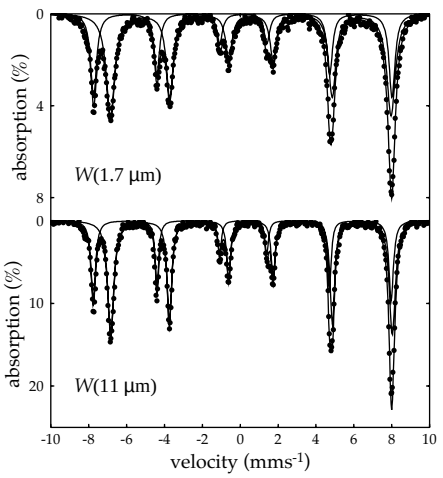

Fig. 1. Room-temperature Mössbauer absorption spectra for samples *W*(1.7 μm) and *W*(11 μm). Two Lorentzian sextets have been fitted to each spectrum. *W*(11 μm) is nearly stoichiometric magnetite, whereas *W*(1.7 μm) is slightly non-stoichiometric. The difference between the two spectra is most clearly seen by comparing the peaks on the extreme left. The difference in absorption percentages is simply due to differences in sample mass.

Table 1
Summary of the grain-size distributions and room-temperature hysteresis parameters for the samples in this study

Sample	Size (μm)		Mean AR	H_c (mT)	H_{cr} (mT)	M_{rs}/M_s
	mean	σ				
W(1.7 μm)	1.7[a]	0.2[a]	1.4	16.1	39.1	0.149
W(7.0 μm)	7[a]	3[a]	1.0	6.2	24.9	0.065
W(11 μm)	11[a]	3[a]	1.8	4.6	20.4	0.044
H(39 μm)	39	9	–	1.2	24.7	0.010
H(108 μm)	108	31	–	0.94	18.2	0.002

The Wright samples had log-normal distributions. These were transformed into $\log_{10}$ space before the mean and standard deviation were calculated. The hydrothermally produced samples displayed a more Gaussian size distribution. σ is the standard deviation of the normal distribution in either case, but σ given in the table for the Wright samples is not symmetric about the mean on a linear scale. The aspect ratio (AR) is the ratio of the long axis over the short axis. No aspect ratio was measured for the hydrothermally produced samples as the grains were nearly all symmetrical. The hysteresis parameters H_c, H_{cr} and M_{rs}/M_s are shown.

[a] Converted from $\log_{10}$ space.

Table 2
Mössbauer parameters of two sextets (A and B) for all three Wright samples

Sample	B_{hf} (T)		QS (mm s^{-1})		IS (mm s^{-1})		Two-phase		
	A	B	A	B	A	B	F_B/F_A	% γ-Fe_2O_3	z
W(1.7 μm)	49.4	46.1	−0.02	−0.02	0.28	0.66	1.67	12	0.045
W(7.0 μm)	49.4	46.2	−0.02	∼0	0.28	0.67	1.71	10	0.039
W(11 μm)	49.5	46.1	∼0	∼0	0.29	0.67	1.86	2.3	0.009

Two of the spectra are shown in Fig. 1 (W(1.7 μm) and W(11 μm)). IS = isomer shift (with reference to metallic iron); QS = quadrupole splitting; B_{hf} = magnetic hyperfine field; F_B/F_A is the ratio of the area of sextets A and B. F_B/F_A is calculated assuming $[Fe_B^{2+}][Fe_A^{3+}Fe_B^{3+}]$. The two-phase model calculation is made assuming two separate stoichiometric phases, magnetite and maghemite. The estimate for z was made by comparing F_B/F_A ratios to those in the literature [17,18].

measuring Mössbauer spectra in the presence of an external field [16]. However, this facility was not available. The two-phase model is relatively straightforward to determine. The oxidation parameter z was determined by comparing the F_B/F_A ratios in Table 2 to the average of the experimental data in Ramdani [17] and Schmidbauer and Keller [18]. The degree of oxidation was found to decrease with grain size. For the two-phase model, the percentage of maghemite was determined to be ≈12% in W(1.7 μm) and only ≈2.3% in W(11 μm). In the cation-deficient model, z drops from 0.045 for W(1.7 μm) to 0.009 for W(11 μm).

The stoichiometry was checked magnetically by examining both the Curie and Verwey temperatures. The Curie temperatures were determined by measuring thermomagnetic curves on a Princeton Measurements vibrating sample magnetometer (VSM). The Curie temperatures were 583 ± 1°C, which is a little above that of stoichiometric magnetite of 575–580°C [19].

The Verwey transition was examined by measuring susceptibility using a Lakeshore Cryotronics AC susceptometer (Fig. 2). The transition was relatively sharp in W(11 μm), indicating near-stoichiometric magnetite, but broader in W(1.7 μm). It is uncertain whether this broadening in the smaller grains is due to differences in stoichiometry and/or grain size.

The second set of samples, H(39 μm) and H(108 μm), were produced by the hydrothermal recrystallisation method [20]. The magnetic properties of these samples have been reported several times previously [7,21]. Grain size distributions and magnetic parameters of the samples are summarised in Table 1. XRD analysis and Mössbauer spectroscopy found that the samples were pure magnetite. The samples were dispersed in KBr pellets, and then vacuum-sealed in quartz capsules. As the samples were stored in vacuum, oxidation was not expected. However, to check, warming curves for an SIRM at 35 K were measured using a Quantum Design MPMS. A very sharp Verwey transition was observed, indicating stoichiometric magnetite.

Magnetic hysteresis parameters were measured at room temperature for all six samples using the VSM (Table 1). The hydrothermally grown samples have very low values for coercive force (H_c) and low saturation remanence (M_{rs}) to M_s ratios, suggesting low dislocation densities. The Wright samples have slightly higher H_c and M_{rs}/M_s values, indicating an increased level of internal stress,

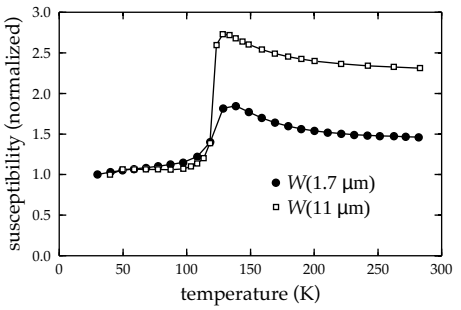

Fig. 2. Low-temperature susceptibility curves for samples W(1.7 μm) and W(11 μm). The susceptibility was measured during warming for two frequencies: 400 Hz and 4000 Hz. No frequency dependence was observed. Only the 400 Hz data are shown. The samples were cooled in zero field.

which may be related to the non-stoichiometry. In addition to the hysteresis properties, first-order reversal curve (FORC) diagrams have been measured for these samples at room temperature [21].

3. Experimental procedures

A series of LTC experiments were made; samples were given either an ARM, pARM or partially demagnetised SIRM, and the behaviour of the remanence was measured during LTC. These experiments were designed to examine how different fractions of the coercivity spectrum behave during LTC.

ARMs and pARMs were induced with a DTech pARM inducer/demagnetiser. The maximum AC field was 200 mT. The effect of applying different biasing DC fields over different field ranges was examined. Partially demagnetised SIRMs were examined by first inducing an SIRM in a field of 1 T using an ASC pulse magnetiser. The samples were then partially demagnetised using the AF demagnetiser.

Low-temperature behaviour of remanence was measured using an MPMS. Before measuring the LTC curves, the internal field inside the MPMS was reduced to ± 0.5 μT. To test the effects of small biasing fields on LTC curves, Muxworthy and McClelland [7] applied fields up to ~ 500 μT during LTC of SIRM. They found that although the field induced a magnetisation which shifted the LTC curves in the direction of the biasing field, the overall behaviour of the low-temperature thermomagnetic curve was not affected, i.e. the jump feature at T_V still existed regardless of the bias field direction. They concluded that small biasing fields of the size ± 0.5 μT were not the cause of the jump behaviour on cooling through T_V.

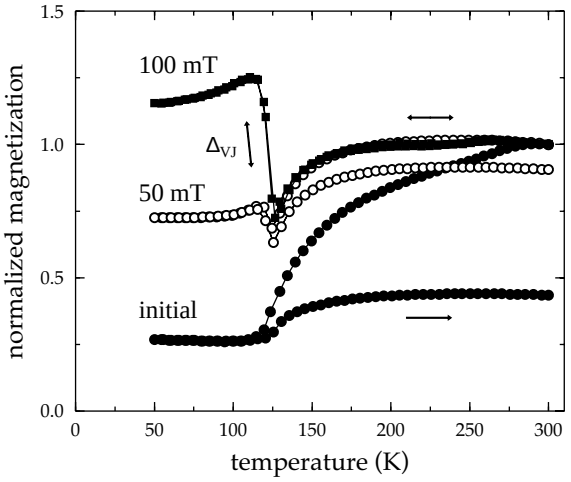

Fig. 3. LTC curves for sample W(7.0 μm) carrying an SIRM, an SIRM AF demagnetised to a maximum field of 50 mT and an SIRM AF demagnetised to 100 mT. The parameter Δ_{VJ} is depicted.

4. Results

4.1. Low-temperature cycling of partially AF-demagnetised SIRMs

For three samples, W(7.0 μm), H(39 μm) and H(108 μm), LTC curves were measured for partially AF-demagnetised SIRMs (Fig. 3). The general shape of the undemagnetised SIRM LTC curves was in good agreement with previously published data for assemblages of PSD and MD magnetite [2–4,7]. As the peak AF demagnetisation field increases, several features are observed. First, the demagnetisation which occurs on cooling to T_K, associated with domain wall re-ordering, decreases. Second, a sudden increase or jump occurs on cooling through T_V for peak AF ≥ 50 mT. Third, the memory ratio, i.e. (memory remanence)/(initial remanence), increases. The width of the Verwey transition was greater in sample W(7.0 μm) than in H(39 μm) and H(108 μm), most likely because of differences in stoichiometry.

The sharp change in magnetisation at T_V is characterised by a new parameter, the 'Verwey jump' (Δ_{VJ}), which is defined as the size of the increase or decrease in magnetisation across the Verwey transition on cooling normalised by the room temperature magnetisation. Specifically, we calculated Δ_{VJ} as the jump in magnetisation over a 10 K interval, starting at T_V and ending 10 K below T_V, divided by the initial magnetisation. Because T_V decreases if magnetite contains impurities or is partially oxidised [9], T_V should be iden-

tified by eye for each individual sample as the temperature at which the magnetisation begins to change sharply. Commonly T_V is associated with a minimum or a 'wild zone' [3] in the temperature range 110–130 K. For all the samples in this study, T_V was at ≈124–125 K. Both positive and negative values for Δ_{VJ} have been previously observed [1,6,7].

The absolute values of the jump, i.e. $\Delta_{VJ} \times$ the initial remanent magnetisation, increase for W(7.0 μm) and H(39 μm), showing a peak at an AF of 50 mT, before decreasing gradually with increasing AF (Fig. 4a). For H(108 μm) the absolute jump size decreases with alternating field. In contrast, Δ_{VJ} is seen to increase as a function of peak AF for samples W(7.0 μm), H(39 μm) and H(108 μm) (Fig. 4b). That is, the relative size of the jump increases with peak AF, suggesting that Δ_{VJ} is associated with the high-coercivity fraction.

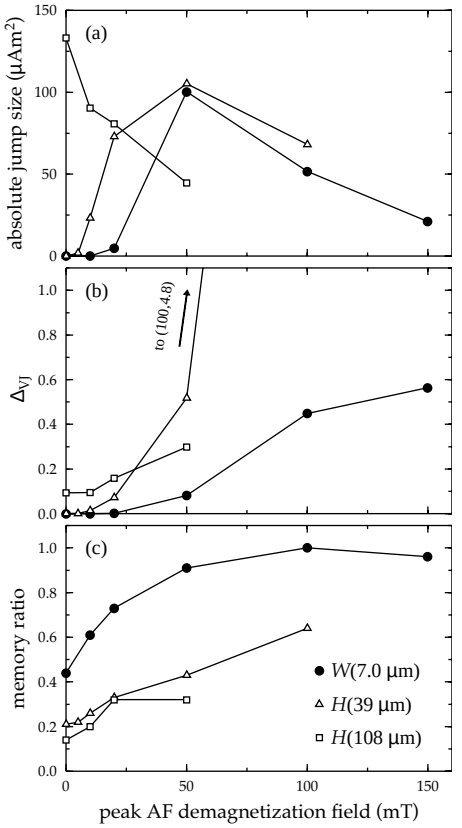

Fig. 4. The absolute jump size (a), Δ_{VJ} (b) and the memory ratio (c) versus the peak AF demagnetisation field for samples W(7.0 μm), H(39 μm) and H(108 μm) induced initially with an SIRM. The relative absolute values for the jump size between the three samples reflect the relative amount of material in each sample. The maximum AF demagnetisation field for H(108 μm) was 50 mT.

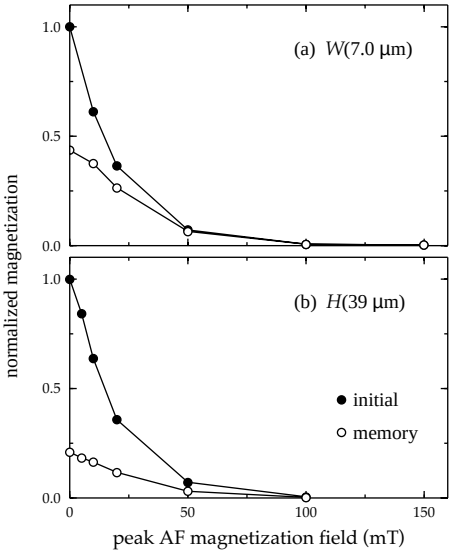

Fig. 5. Simulated AF demagnetisation curves of initial SIRM and SIRM memory for samples (a) W(7.0 μm) and (b) H(39 μm). Before each AF demagnetisation step a new SIRM was produced. H(108 μm) displayed similar behaviour to H(39 μm).

The memory ratio is also seen to increase with peak AF (Fig. 4c), supporting the idea that the high-coercivity component of remanence displays reversible behaviour to LTC [7]. The AF-demagnetised memory ratio increases with peak AF for W(7.0 μm), reaching a value of 1 at 100 mT.

From the complete data set for each sample, it is possible to construct standard AF demagnetisation curves for both initial remanence and memory (Fig. 5). The initial remanence is more easily demagnetised than its memory until some AF level is reached where the two AF demagnetisation curves become identical. Similar contrasts between AF demagnetisation curves of initial remanence and memory have been reported previously [7,22–24].

4.2. Low-temperature cycling of pARM

LTC curves were measured for pARM induced

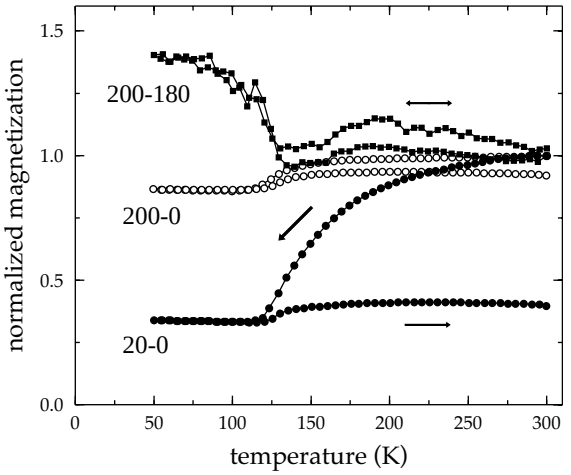

Fig. 6. LTC curves for W(1.7 μm) with pARMs induced over three different ranges: $pARM_0^{200}$ (= ARM in other diagrams), $pARM_{180}^{200}$ and $pARM_0^{20}$. The peak AF during pARM acquisition was 200 mT, and the DC field was set to 200 μT.

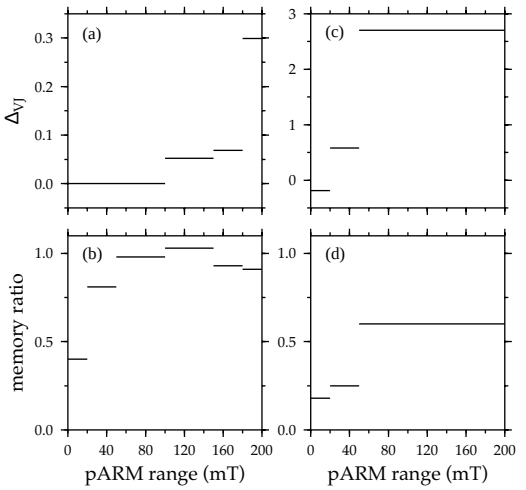

Fig. 7. Δ_{VJ} and the memory ratio versus pARM inducing field range for different pARMs in samples W(1.7 μm) (a,b) and H(39 μm) (c,d). W(1.7 μm) had six pARMs induced over the 200 mT range, whilst H(39 μm) had three. The corresponding Δ_{VJ} values and memory ratios for a complete ARM were 0% and 92% for W(1.7 μm) and 35% and 4% for H(39 μm).

in samples W(1.7 μm) and H(39 μm) using a DC field of 200 μT (Fig. 6). The maximum AF was always set to 200 mT. Δ_{VJ} and the memory ratios increased with the AF field range over which the pARM was induced for both W(1.7 μm) and H(39 μm) (Figs. 6 and 7). For $pARM_0^{20}$, i.e. a pARM induced between AFs of 20 and 0 mT, Δ_{VJ} for H(39 μm) was observed to be negative. Negative Δ_{VJ} values have been observed before for various types of TRMs induced in large MD magnetites [1,7]. That Δ_{VJ} is a maximum for high AF ranges supports the idea that Δ_{VJ} is related to the high-coercive-force fraction.

For sample W(1.7 μm), the memory ratio for $pARM_0^{20}$ is smaller than the ARM memory ratio, i.e. $pARM_0^{200}$. The ratios were 40% and 92% respectively, supporting the idea that low-temperature demagnetisation is related to the low-coercivity fraction as suggested by Figs. 3 and 4. H(39 μm) displayed different behaviour, and the memory ratios for $pARM_0^{20}$ and ARM were, respectively, 18% and 4%. It is unclear why the memory ratio for ARM was less than any of the pARM memory ratios (Fig. 7).

From the pARM data it is possible to determine remanence acquisition distributions. For W(1.7 μm) the peak in the distribution was for $pARM_{20}^{50}$, whereas H(39 μm) displayed a maximum in the distribution at low-field ranges, i.e. $pARM_0^{20}$. These correspond well with cross-sections of the FORC distribution along the H_C-

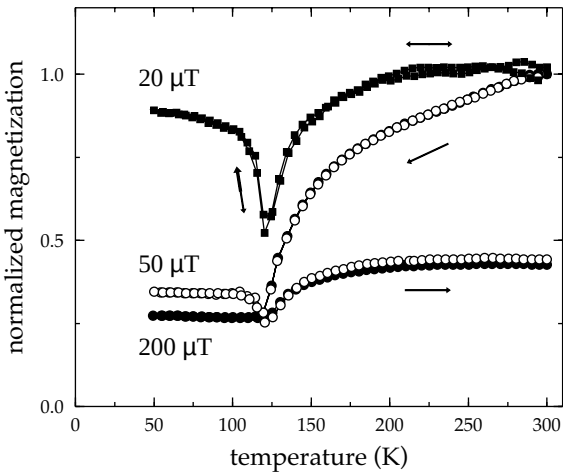

Fig. 8. LTC curves for W(11 μm) with ARMs induced in three different DC fields (20, 50 and 200 μT). The peak AF during ARM acquisition was 200 mT. The cooling curves for the 50 μT and 200 μT remanences overlap each other.

axis (x-axis) reported in Muxworthy and Dunlop [21].

4.3. Effect of ARM acquisition field on LTC behaviour

In Fig. 8, LTC curves for W(11 μm) are shown for ARMs produced with a range of DC fields. As the DC biasing field increases, the shape of the LTC curves evolves, with Δ_{VJ} decreasing (Fig. 9). For the larger DC fields, ARM LTC curves resembled SIRM LTC curves (Fig. 3). The memory ratio also decreases with DC field (Fig. 9). This field-dependent behaviour is similar to that observed for TRM [7].

ARM and ARM memory acquisition curves were linear with applied field up to 200 μT, in agreement with Muxworthy and McClelland [7], who measured such linear trends for acicular SD magnetite, and hydrothermal and natural MD magnetite.

LTC curves for ARM induced in samples W(1.7 μm) and W(7.0 μm) in a DC field of 200 μT displayed similar behaviour to W(11 μm) (Fig. 8), i.e. $\Delta_{VJ} = 0$. The memory ratio gradually decreased with grain size, i.e. 92%, 47% and 31% for samples W(1.7 μm), W(7.0 μm) and W(11 μm), respectively. It is uncertain what contribution the differences in stoichiometry made to these memory ratios.

4.4. Reversibility of ARM LTC

To check for reversibility, an ARM (DC field = 200 μT) was induced in sample W(11 μm) at room temperature and the remanence gradually cycled between room temperature and increasingly lower temperatures (Fig. 10). The induced ARM is seen to partially demagnetise on cooling to temperatures $> T_V$ and T_K, e.g. cooling to 150 K is sufficient to demagnetise 22% of the initial ARM on warming to room temperature. Similar data have been reported for low-temperature cycled SIRM [4,7]. This result strongly supports the theory that domain wall re-organisation during cooling above T_K is a major contributor to the total low-temperature demagnetisation. On cooling through T_V, the memory ratio is seen to drop sharply, indicating that significant demagnetisation occurs on cooling through T_K and T_V.

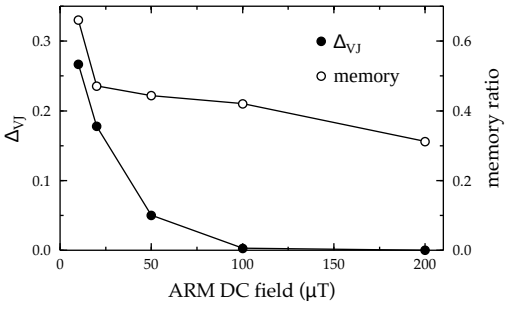

Fig. 9. Δ_{VJ} and the memory ratio versus ARM DC acquisition field for sample W(11 μm). Δ_{VJ} was zero for high fields. The peak AF during ARM acquisition was 200 mT.

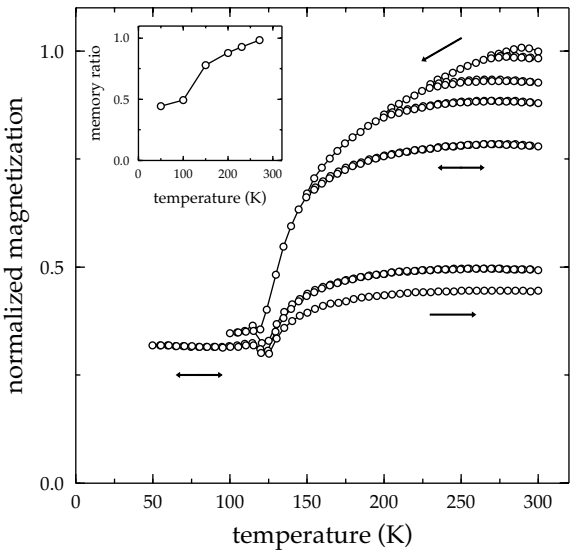

Fig. 10. Low-temperature cycling curves for W(11 μm) induced with an initial ARM (DC field = 200 μT). The sample was cycled from room temperature to a series of gradually decreasing temperatures. The inset shows the memory ratio as a function of minimum temperature reached after each LTC cycle.

5. Discussion

There are large variations in both the initial remanences and LTC curves shown in this paper.

However, there are two clear trends. First, initial remanences associated with higher-coercivity fractions display the highest Δ_{VJ} values, e.g. Δ_{VJ} is largest for SIRM AF-demagnetised to 100 mT (Fig. 3) and $pARM_{180}^{200}$ (Fig. 6). Secondly, the high-coercivity fraction is generally reversible during LTC, i.e. the high-coercivity remanences have the highest memory ratios (Figs. 4 and 7). Irreversible behaviour is observed when the lower-coercivity fraction of remanence is present.

Δ_{VJ} displays a grain-size dependence (Figs. 4 and 7). Δ_{VJ} for H(39 μm) and H(108 μm) is greater than Δ_{VJ} for W(1.7 μm) for all peak AFs of SIRM. However, as the peak AF increases, Δ_{VJ} for H(39 μm) becomes greater than Δ_{VJ} for H(108 μm) (Fig. 4). Δ_{VJ} for all the pARMs is greater for H(39 μm) than W(1.7 μm) except for the $pARM_0^{20}$ Δ_{VJ}, which is negative for H(39 μm) and zero for W(1.7 μm).

The memory ratio displays a consistent grain-size dependence (Figs. 4c and 9). Such grain-size dependence of the memory fraction is well documented for other types of remanence [22,23,25].

Δ_{VJ} decreases strongly with increasing ARM DC field (Fig. 9). The memory ratio displays a weaker dependence on ARM DC field. Muxworthy and McClelland [7] observed a similar field dependence of Δ_{VJ} for pTRM induced in hydrothermally grown MD magnetites for fields between 100 μT and 5 mT. They related the LTC behaviour of the high-field remanence to a shift in domain structure to a more SIRM-like structure. SIRM structures generally have smaller Δ_{VJ} values [5,7]. Δ_{VJ} for an initial SIRM was zero for Wright sample W(1.7 μm), although for some samples Δ_{VJ} SIRM >0, e.g. H(108 μm) (Fig. 4b). Drawing together the results in this study, the effect of decreasing the ARM DC field is to increase the relative size of the high-coercivity fraction of remanence.

5.1. Origin of Δ_{VJ}

In previous papers, simple mutually compatible models were developed to explain positive Δ_{VJ} behaviour [5–8]. Δ_{VJ} was attributed to both a shift to a more SD-like domain state and the removal of closure-like domains in the monoclinic phase [5,7,8].

The shift in domain state is related to the large increase in the magnetocrystalline anisotropy on cooling through T_V, causing the SD/MD threshold size to increase [5,8]. On cooling through T_V the domain structure tries to denucleate walls, or at least re-equilibrate walls to reduce the total energy. This will on average increase the measured magnetisation of a sample. Generally, denucleation of domain walls is thought to be irreversible, whilst wall re-equilibration is reversible.

That the isolated high-coercive-force fraction of remanence displays reversible behaviour at T_V suggests that its behaviour is controlled by domain wall re-equilibration processes (e.g. Figs. 3 and 6).

The contribution of removing closure domains to Δ_{VJ} is more debatable, especially for small PSD grains. Closure domains have been clearly observed in large MD magnetite [26]. In small PSD magnetite such features are generally not observed [27,28]. However, grain-edge features which reduce the magnetic flux leakage in PSD magnetite are predicted to exist and to be difficult to observe experimentally [29]. On simulated cooling through the Verwey transition, the removal of such features was the main contributor to Δ_{VJ} [5].

The high-coercive-force fraction of remanence is more likely than the low-coercive-force fraction to be associated with domain configurations where domain walls are pinned far from their equilibrium positions. To reduce the energy of these states in the cubic phase, closure domains are likely to form. The removal of such closure domains will result in an increase in Δ_{VJ}. Experimentally, Δ_{VJ} becomes relatively larger as the higher coercive fraction becomes increasingly isolated (Figs. 4 and 7).

The relative increase in Δ_{VJ} from both of these effects will be greater for small grains, e.g. reducing a domain structure from two domains to a SD will lead to a bigger increase in Δ_{VJ} than decreasing from, say, 20 domains to 18, and the importance of closure domains is also greater for domain structures with only a few domains. In contrast, the results in this paper show that Δ_{VJ}

increases with grain size (Figs. 4 and 7). This discrepancy may be due to the very different microcoercivity distributions of the Wright and hydrothermal samples; the influence of microcoercivity may mask the expected grain-size trend. Özdemir et al. [8] found a similar grain-size relationship for SIRMs, whereas Muxworthy and McClelland [7] found that Δ_{VJ} for TRM increased as the grain size was decreased.

In addition to these two mechanisms, twin domain (TD) structures are thought to be important to the low-temperature magnetic behaviour due to the high magnetocrystalline anisotropy [6–8]. However, it is difficult to assess their importance as certain key facts are unknown. Firstly, there may or may not be TD boundaries as there is a single-TD to multi-TD critical size [30,31]. The critical size depends on the boundary conditions of each grain, and it is not possible to roughly estimate the critical size as this is a highly nonlinear calculation (A. Jacobs, personal communication, 2002). Secondly, the interaction of remanence structures with TDs is unknown. Either the twin or the magnetic domains could dominate the remanence behaviour depending on whether the strain or magnetic energy dominates (A. Jacobs, personal communication, 2002). In addition, it is possible due to the symmetry considerations, for certain orientations of TD and magnetic domain walls to re-adjust independently (C. Medrano, personal communication, 1999).

5.2. Origin of high memory ratios

High memory ratios reflect reversible behaviour through the entire LTC curve, including on cooling through T_V (Figs. 3, 6 and 8). Irreversible behaviour is thought to be due to denucleation of domain walls, both on cooling from room temperature to T_K due to the decrease in the magnetocrystalline anisotropy (Fig. 10), and on cooling to below T_V. High memory ratios were found to be related to high coercivity remanences (Figs. 4 and 7). This is in agreement with AF demagnetisation curves of both initial and memory remanence (Fig. 5, [7,22,23]). These high-coercivity remanences are more likely to be stress-controlled, and hence relatively unaffected by changes in the magnetocrystalline anisotropy. When palaeomagnetic remanences are thermally demagnetised, a magnetoelastically controlled remanence decays much less rapidly than a magnetocrystalline controlled one. Thus a high memory ratio, implying magnetoelastic control, is likely to be an indicator of a palaeomagnetically meaningful remanence with high unblocking temperatures.

6. Conclusions

This study clearly demonstrates that LTC behaviour is influenced by the coercive force distribution of the remanence. It is shown that key features such as Δ_{VJ} and high memory ratios are associated with the highest coercivity fraction of remanence. Some of the LTC behaviour can be explained by the application of previously reported theories [5–8].

The identification of high memory ratios or a significant Δ_{VJ} peak for a natural remanent magnetisation (NRM) would indicate that the remanence was dominated by a magnetoelastically controlled high coercivity signal, and that the sample is suitable for palaeomagnetic investigations. The measurement of memory ratio does not require low-temperature measurements of magnetisation. It is recommended that LTC be used as a preselection technique in palaeomagnetic studies, and if applied judiciously it could be used as a cleaning technique [32].

In addition, LTC analysis can be used to identify the domain state dominating the NRM signal in magnetite-bearing rocks; high memory ratios and large jumps at the Verwey transition indicate a high-coercive force MD remanence, high memory ratios and small jumps at the Verwey transition suggest an SD remanence, whilst low-memory ratios indicate a low-coercive force MD remanence.

Acknowledgements

We benefited from fruitful discussions with Yongjae Yu and Allan Jacobs. Mike Jackson and an anonymous reviewer made constructive

comments. We thank Wright Industries for providing the samples. Fred Neub of the Materials Engineering Department, University of Toronto, helped with the SEM work. The magnetic experiments were made at the Institute for Rock Magnetism, University of Minnesota, which is funded by the National Science Foundation, the W.M. Keck Foundation and the University of Minnesota. We thank Mike Jackson, Peat Sølheid and Jim Marvin for help with the measurements. This research has been supported by the Natural Sciences and Engineering Research Council of Canada through Grant A7709 to D.J.D.*[AV]*

References

[1] M. Ozima, M. Ozima, S.-T. Akimoto, Low-temperature characterisation of remanent magnetisation of magnetite - self-reversal and recovery phenomena, J. Geomagn. Geoelectr. 16 (1964) 165–177.

[2] K. Kobayashi, M. Fuller, Stable remanence and memory of multidomain materials with special reference to magnetite, Philos. Mag. 18 (1968) 601–624.

[3] S.L. Halgedahl, R.D. Jarrard, Low temperature behaviour of single domain through multidomain magnetite, Earth Planet. Sci. Lett. 130 (1995) 127–139.

[4] J.P. Hodych, R.I. Mackay, G.M. English, Low-temperature demagnetization of saturation remanence in magnetite-bearing dolerites of high coercivity, Geophys. J. Int. 132 (1998) 401–411.

[5] A.R. Muxworthy, W. Williams, Micromagnetic models of pseudo-single domain grains of magnetite near the Verwey transition, J. Geophys. Res. 104 (1999) 29203–29218.

[6] Ö. Özdemir, D.J. Dunlop, Low-temperature properties of a single crystal of magnetite orientated along principal magnetic axes, Earth Planet. Sci. Lett. 165 (1999) 229–239.

[7] A.R. Muxworthy, E. McClelland, The causes of low-temperature demagnetisation of remanence in multidomain magnetite, Geophys. J. Int. 140 (2000) 115–131.

[8] Ö. Özdemir, D.J. Dunlop, B.M. Moskowitz, Changes in remanence, coercivity and domain state at low temperature in magnetite, Earth Planet. Sci. Lett. 194 (2002) 343–358.

[9] A.R. Muxworthy, E. McClelland, Review of the low-temperature magnetic properties of magnetite from a rock magnetic perspective, Geophys. J. Int. 140 (2000) 101–114.

[10] R.J. Harrison, Magnetic transitions in minerals, in: S.A.T. Redfern, M.A. Carpenter (Eds.), Reviews in Mineralogy and Geochemistry, Vol. 39 – Transformation Processes in Minerals, Mineralogical Society of America, Washington, DC, 2000, pp. 175–202.

[11] J. King, W. Williams, Low-temperature properties of magnetite, J. Geophys. Res. 105 (B7) (2000) 16427–16436.

[12] R.L. Hartstra, TRM, ARM and Isr of two natural magnetites of MD and PSD grain size, Geophys. J. R. Astron. Soc. 73 (1983) 719–737.

[13] B. Carter-Stiglitz, M. Jackson, B.M. Moskowitz, Low-temperature remanence in stable single domain magnetite, Geophys. Res. Lett. 10.1029/2001GL014197 (2002) 437–450.

[14] A. Hubert, R. Schäfer, Magnetic Domains, Springer, Berlin, 1998.

[15] Y. Yu, D.J. Dunlop, Ö. Özdemir, Partial anhysteretic remanent magnetization in magnetite 1. Additivity, J. Geophys. Res. 107 (B10), 101029/2001JB001269.

[16] R.E. Vandenberghe, C.A. Barrero, G.M. Da Costa, E. Van San, E. De Grave, Mössbauer characterization of iron oxides and (oxy)hydroxides: the present state of the art, Hyperfine Interact. 126 (2000) 247–259.

[17] A. Ramdani, J. Steinmetz, C. Gleitzer, J.M. Coey, J.M.D. Friedt, Perturbation de l'échange électronique rapide par les lacunes cationiques dans $Fe_{3-x}O_4$ ($x \leq 0.09$), J. Phys. Chem. Solids 48 (1987) 217–228.

[18] E. Schmidbauer, R. Keller, Magnetic hysteresis properties, ^{57}Fe Mössbauer spectra and structural data of spherical 250 nm particles of solid solutions Fe_3O_4-γ-Fe_2O_3, J. Magn. Magn. Mater., submitted.

[19] D.J. Dunlop, Ö. Özdemir, Rock Magnetism: Fundamentals and Frontiers, Cambridge University Press, 1997.

[20] F. Heider, L.T. Bryndzia, Hydrothermal growth of magnetite crystals (1 μm to 1 mm), J. Cryst. Growth 84 (1987) 50–56.

[21] A.R. Muxworthy, D.J. Dunlop, First-order reversal curve (FORC) diagrams for pseudo-single-domain magnetites at high temperature, Earth Planet. Sci. Lett. 203 (2002) 369–382.

[22] D.J. Dunlop, K.S. Argyle, Separating multidomain and single-domain-like remanences in pseudo-single-domain magnetites (215–540 nm) by low-temperature demagnetisation, J. Geophys. Res. 96 (1991) 2007–2017.

[23] E. McClelland, V.P. Shcherbakov, Metastability of domain state in MD magnetite: consequences for remanence acquisition, J. Geophys. Res. 100 (1995) 3841–3857.

[24] Ö. Özdemir, D.J. Dunlop, Single-domain-like behavior in a 3-mm natural single crystal of magnetite, J. Geophys. Res. 103 (1998) 2549–2562.

[25] F. Heider, D.J. Dunlop, H.C. Soffel, Low temperature and alternating field demagnetisation of saturation remanence and thermoremanence in magnetite grains (0.037 μm to 5 mm), J. Geophys. Res. 97 (B6) (1992) 9371–9381.

[26] Ö. Özdemir, S. Xu, D.J. Dunlop, Closure domains in magnetite, J. Geophys. Res. 100 (1995) 2193–2209.

[27] C.E. Geiss, F. Heider, H.C. Soffel, Magnetic domain ob-

servations on magnetite and titanomaghemite grains (0.5–10 μm), Geophys. J. Int. 124 (1996) 75–88.
[28] T.G. Pokhil, B.M. Moskowitz, Magnetic domains and domain walls in pseudo-single-domain magnetite studied with magnetic force microscopy, J. Geophys. Res. 102 (1997) 22681–22694.
[29] W. Williams, T.M. Wright, High resolution micromagnetic models of fine grains of magnetite, J. Geophys. Res. B 12 (1998) 30537–30550.
[30] E.K.H. Salje, Ferroelasticity, Cont. Phys. 41 (2000) 79–91.
[31] W. Cao, C.A. Randall, Grain size and domain size relations in bulk ceramic ferroelectric materials, J. Phys. Chem. Solids 57 (1996) 1499–1505.
[32] M. Ozima, M. Ozima, T. Nagata, Low-temperature treatment as an effective means of 'magnetic cleaning' of natural remanent magnetisation, J. Geomagn. Geoelectr. 16 (1964) 37–41.